Received 14 August 2024; revised 13 September 2024; accepted 15 September 2024. Date of publication 24 September 2024; date of current version 3 October 2024. The review of this article was arranged by Editor C.-H. Kim.

Digital Object Identifier 10.1109/JEDS.2024.3466956

Performance Enhancement of Indium Zinc Oxide Thin-Film Transistors Through Process Optimizations

MINGJUN ZHANG[1], JINYANG HUANG[1], ZIHAN WANG[1], PARAMASIVAM BALASUBRAMANIAN[2,3], YAN YAN[2,3], YE ZHOU[4], SU-TING HAN[5], LEI LU[6] (Member, IEEE), AND MENG ZHANG[2,3] (Senior Member, IEEE)

1 Institute of Microscale Optoelectronics, Shenzhen University, Shenzhen 518060, China
2 State Key Laboratory of Radio Frequency Heterogeneous Integration, Shenzhen University, Shenzhen 518060, China
3 College of Electronics and Information Engineering, Shenzhen University, Shenzhen 518060, China
4 Institute for Advanced Study, Shenzhen University, Shenzhen 518060, China
5 Department of Applied Biology and Chemical Technology, The Hong Kong Polytechnic University, Hong Kong, China
6 School of Electronic and Computer Engineering, Shenzhen Graduate School, Peking University, Shenzhen 518055, China

CORRESPONDING AUTHOR: M. Zhang (e-mail: zhangmeng@connect.ust.hk)

This work was supported in part by the Shenzhen Municipal Research Program under Grant SGDX20211123145404006; in part by the National Natural Science Foundation of China under Grant 62274111; in part by the Innovation and Technology Fund of Hong Kong under Grant GHP/018/21SZ; in part by the National Taipei University of Technology–Shenzhen University Joint Research Program under Grant 2024004; and in part by the Independent Scientific Research Program from State Key Laboratory of Radio Frequency Heterogeneous Integration under Grant 2024015.

ABSTRACT The device performance of indium zinc oxide (IZO) thin-film transistors (TFTs) is optimized through process optimizations. By jointly adjusting the annealing condition, the channel thickness and the sputtering atmosphere, the roughness and oxygen vacancies (V_os) are precisely regulated. The optimized IZO TFTs can achieve the highest field effect mobility of ~71.8 cm^2/Vs with a threshold voltage of ~–0.6 V. Reliability of IZO TFTs under positive/negative bias stress is also examined. The interface quality and the V_os are two key factors influencing the device performance and reliability, confirmed by X-ray photoelectron spectroscopy and atomic force microscopy analysis.

INDEX TERMS InZnO, thin-film transistors, magnetron sputtering, process optimization.

I. INTRODUCTION

Due to the decent mobility (μ) and cost-effective manufacturing processes, metal oxide (MO) semiconductors are commonly employed as alternatives to amorphous silicon in the active layer of thin-film transistors (TFT) for active matrix (AM) displays [1]. Among the numerous MO semiconductors, indium-gallium-zinc oxide (IGZO) was the first to achieve successful commercialization, due to its excellent balance between device performance and reliability. However, as carrier inhibitors, the presence of gallium (Ga) inhibits the generation of oxygen vacancies (V_os), greatly limiting the carrier mobility of the device [2], [3]. Thus, the μ of IGZO TFT is usually ~10 cm^{2}V^{-1}s^{-1} [4], rendering them inadequate for meeting the demands of the new generation of AM displays with high definition and high refresh rate.

By replacing the carrier inhibitor element Ga with some other metal elements, such as tin (Sn) [5] or tungsten (W) [6], the film is expected to improve the μ [5], [6] or reliability [5], [6]. When Ga in IGZO is replaced by chemically stable Sn, the direct spatial overlap between the Sn 5s orbital and the indium (In) 5s orbital induces higher conduction band electron μ [7]. When Ga is replaced by W, due to its higher oxygen bond dissociation energy than Ga [8], it can better suppress the generation of oxygen-related defects and improve device reliability. However, all of the above improvements are still not enough for high-definition AM displays with high refresh rate. By removing the Ga, Sn, or W, indium-zinc oxide (IZO) TFTs [9], which are usually used as phototransistors, can actually be a kind of candidate material for high μ TFTs with lower fabrication cost.

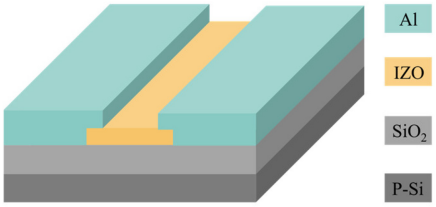

FIGURE 1. Device structure of IZO TFT.

IZO thin film can be fabricated through a variety of techniques, such as radio frequency (RF) magnetron sputtering [2], [3], laser pulse deposition [10], solution-based methods [1], atomic layer deposition [11], inkjet printing [12], and others. Among these techniques, RF magnetron sputtering is the most reliable technology, which is widely adopted in industrial production lines. For RF magnetron-sputtered IZO TFTs, several efforts have been devoted to optimizing device performance through meticulous process refinements, encompassing modulation of IZO thickness [13], [14], fine-tuning of the sputtering atmosphere [15], and management of the annealing process [16]. However, all the studies merely scrutinize the impact of singular alterations in conditions on device performance. Regarding IZO thickness modulation, the optimum μ is ~38 cm^2/Vs with a corresponding threshold voltage (V_{th}) of ~10 V [13]. Concerning sputtering atmosphere tuning, the optimum μ is ~24 cm^2/Vs with a corresponding V_{th} of ~1 V [15]. As for the annealing process control, the optimum μ is ~41 cm^2/Vs with a corresponding V_{th} of ~ –12 V [16]. Although a single optimization strategy can relatively enhance the μ of the device, it also brings about a significant deviation of the V_{th} from 0 V [13], [16]. The joint optimization approach may offer a solution to this issue.

In this work, a joint process optimization strategy was employed to enhance the performance of IZO TFTs. By optimizing the annealing condition, the active layer thickness and the RF magnetron sputtering atmosphere, high-performance IZO TFTs with a field effect mobility (μ_{FE}) of ~71.8 cm^2/Vs and a V_{th} of –0.6 V are successfully achieved. Such improvement is confirmed to be attributed to the good interface and the reasonable regulation of V_os, as characterized by atomic force microscopy (AFM) and X-ray photoelectron spectroscopy (XPS) analysis of the active layer properties. Moreover, both positive bias stress (PBS) and negative bias stress (NBS) tests were conducted on the devices to investigate the impact of IZO thickness and the RF magnetron sputtering atmosphere on device reliability. This joint optimization strategy is expected to provide innovative solutions and valuable insights for advancing the development of high-definition AM displays that incorporate IZO TFTs.

II. EXPERIMENTAL

As illustrated in Fig. 1, the devices in this study feature a bottom-gate and top-contact configuration, with a heavily doped P-type silicon (P-Si) substrate as the bottom gate electrode. A 100 nm thick layer of silicon dioxide is utilized as the gate insulator, grown on top of the substrate. The IZO thin-film was achieved by RF magnetron sputtering method. The target utilized for RF magnetron sputtering is an indium oxide (In_2O_3)/zinc oxide (ZnO) target with a weight ratio of 90/10, corresponding to 90 wt% In_2O_3 and 10 wt% ZnO. The RF magnetron sputtering power and the process pressure were respectively fixed at 60 W and 3 mTorr. To adjust the IZO thickness, the sputtering time was varied while maintaining a fixed Ar/O_2 gas flow ratio of 30/20 sccm in the sputtering atmosphere. A range of five distinct IZO thickness was achieved through this process: 4.8 nm, 9.7 nm, 14.5 nm, 24 nm, and 36 nm. In the optimization of the RF magnetron sputtering atmosphere, five sets of Ar/O_2 ratios were evaluated with the IZO thickness held constant at 14.5 nm. These ratios were Ar/O_2 = 20/30 sccm, 30/20 sccm, 35/15 sccm, 40/10 sccm, and 50/0 sccm, respectively. Following the patterning of the active layer, the source and drain electrodes were fabricated using DC magnetron sputtering of aluminum (Al). The DC magnetron sputtering process utilized a 99.999% high-purity Al target. The sputtering power was set at 120 W, the process pressure was maintained at 4.8 mTorr, and the sputtering time was 250 s. The thickness of Al is 222 nm. After the source/drain electrodes were deposited, the devices were annealed at 200 °C for 10 minutes in an air atmosphere.

The channel width is 500 μm and the channel length is 200 μm. The transfer curve and P/NBS reliability are characterized using a Keysight B1500A semiconductor parameter analyzer connected to a probe station. All tests were conducted in an air atmosphere and at room temperature of 25 °C. The positive and negative gate bias stress voltages are respectively set to +20 V and –20 V. The μ_{FE} is extracted from the transfer curve as described in [17]. The V_{th} in this work is defined as the gate-source voltage (V_{gs}) at which a drain current (I_{ds}) reaches 1 nA. The film thickness was measured by a stylus profilometer (DEKTAK XT). The morphologies roughness of the film was measured by AFM (Bruker MultiMode8). The composition and chemical state of the films were characterized by XPS (Thermo Scientific Nexsa).

III. RESULTS AND DISCUSSION

In this study, by employing a joint process optimization strategy, the IZO TFT with an IZO thickness of 14.5 nm and a sputtering atmosphere of Ar/O_2 = 30/20 sccm demonstrates the highest recorded μ_{FE} of ~71.8 cm^2/Vs, with its V_{th} closest to 0 V at ~–0.6 V. The comparison with the other works on IZO-related TFTs [1], [3], [18], [19], [20], [21], [22], [23], [24], [25] is shown in Fig. 2. Apparently, the optimized IZO TFT in this work demonstrates superior performance.

The optimization process is structured into three segments: annealing conditions, IZO thickness, and sputtering

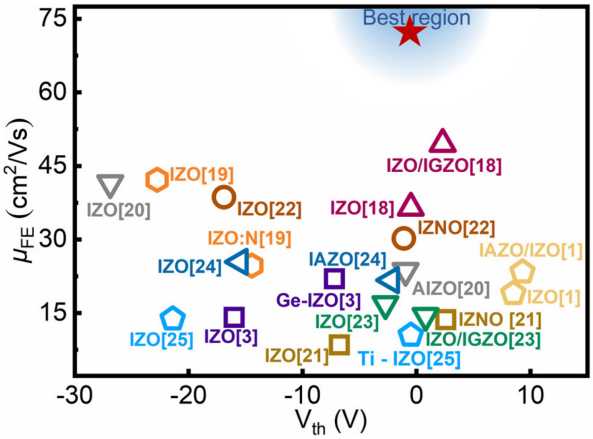

FIGURE 2. Comparison of IZO TFTs manufactured in this work with the other works.

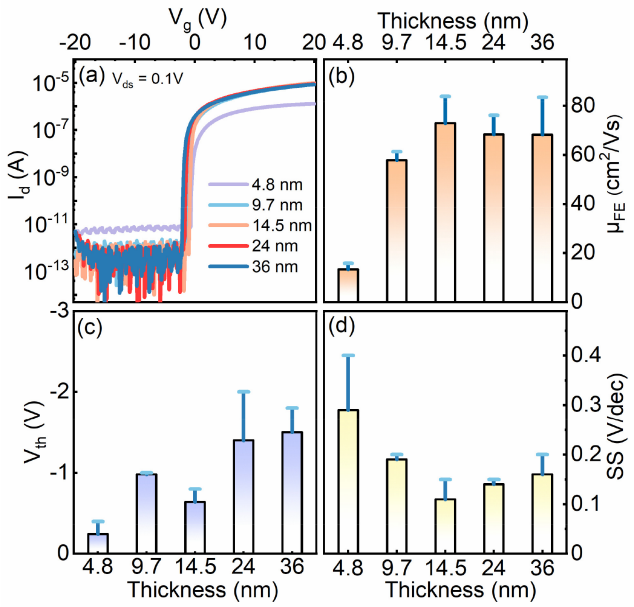

FIGURE 3. Comparison of (a) transfer curve, (b) μ_{FE}, (c) V_{th} and (d) *SS* of IZO TFTs with different IZO thicknesses.

atmosphere. Drawing from extensive experiments, it was discovered that the device consistently displayed stable and uniform performance when subjected to annealing conditions of 200 °C for 10 minutes. Therefore, for the optimization of IZO thickness and sputtering atmosphere, the annealing condition is fixed. Furthermore, the thickness of the active layer significantly affects the I_{on} of the device, but has a relatively minor impact on the V_{th} and *SS*. Conversely, the sputtering atmosphere has a significant impact on the V_{th}, while its influence on I_{on} and *SS* is relatively minor.

IZO thickness optimization was conducted with a fixed sputtering atmosphere of $Ar/O_2 = 30/20$ sccm. The thickness of the IZO active layer varies from 4.8 nm to 36 nm by adjusting the sputtering time from 200 s to 1500 s. The results are shown in Fig. 3. Shown in Fig. 3a is the transfer curve comparison among IZO TFTs with different IZO thicknesses. It can be observed that the IZO thickness has a significant impact on I_{on} compared to its impact on V_{th} and *SS*.

Fig. 3b shows the extracted μ_{FE} of IZO TFTs with different IZO thicknesses. As the IZO thickness increases from 4.8 nm to 14.5 nm, the μ_{FE} gradually increases. Particularly noteworthy is the significant improvement in μ_{FE} observed as the IZO thickness increases from 4.8 nm to 9.7 nm. When the IZO thickness is 14.5 nm, the highest μ_{FE} can reach ~83.9 $cm^2V^{-1}s^{-1}$. Beyond 14.5 nm, despite further increases in the IZO thickness, the μ_{FE} no longer increases and may even slightly decrease. When the IZO thickness is thin, insufficient charge carriers exist within the channel to establish an effective conductive path, thus constraining μ_{FE} to a low level. However, when the active layer surpasses a critical thickness, it can supply adequate carriers for device operation, diminishing carrier content as the primary factor restricting μ_{FE} increase. Consequently, device μ_{FE} reaches a saturation state. In addition, previous studies [13], [26] have shown that the roughness of the interface also impacts carrier transport.

Fig. 3c shows the corresponding V_{th} extracted from devices with different IZO thicknesses. As the thickness of the active layer increases from 4.8 nm to 36 nm, the V_{th} of the device gradually deviates from 0 V, exhibiting a negative offset trend. Among all devices, the optimal V_{th} is 0 V. The variation in IZO thickness may affect the V_{th} of the device by altering the carrier content. As the thickness of the active layer increases, the number of carriers may also increase, facilitating the accumulation of free carriers in the transport layer and making the devices easier to operate [27].

Fig. 3d shows the extracted *SS* of IZO TFTs with different IZO thicknesses. As the IZO thickness increases, the *SS* initially decreases and then increases. An optimal IZO thickness can maintain *SS* in a relatively ideal state, whereas excessive or insufficient IZO thickness can deteriorate *SS*. The deterioration of *SS* due to large IZO thickness can be explained by an increase in trap density and a decrease in effective capacitance at the interface [13], [14], [28]. For devices with thinner active layers, the degradation of *SS* may result from the carrier transport layer being close to the surface, which amplifies the impact of interface defects on the device [13], [14].

Sputtering atmosphere optimization was conducted at IZO thickness of 14.5 nm. The sputtering atmospheres used were Ar/O_2 = 20/30 sccm, 30/20 sccm, 35/15 sccm, 40/10 sccm, and 50/0 sccm. The results are shown in Fig. 4. Fig. 4a compares the transfer curves of IZO TFTs with different sputtering atmospheres. When the sputtering atmosphere is Ar/O_2 = 50/0 sccm, the device no longer exhibits the characteristics of a TFT, so it is not shown in the figure. It can be observed that the sputtering atmosphere has a significant impact on V_{th}, compared to its relatively minor impact on I_{on} and *SS*.

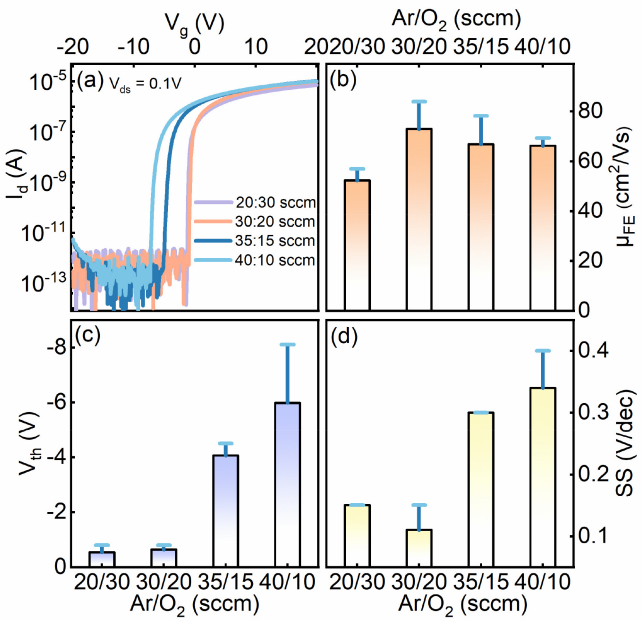

FIGURE 4. Comparison of (a) transfer curve, (b) μ_{FE}, (c) V_{th} and (d) *SS* of IZO TFTs fabricated at different sputtering atmospheres.

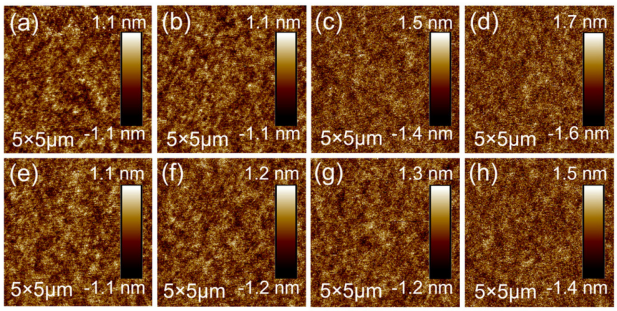

FIGURE 5. AFM images of IZO thin film with (a) IZO thickness of 4.8 nm, (b) IZO thickness of 9.7 nm, (c) IZO thickness of 24 nm, and (d) IZO thickness of 36 nm. AFM images of IZO thin film fabricated at (e) Ar/O_2 = 20/30 sccm, (f) Ar/O_2 = 30/20 sccm, (g) Ar/O_2 = 35/15 sccm, and (h) Ar/O_2 = 40/10 sccm.

Fig. 4b shows the extracted μ_{FE} of IZO TFTs with different sputtering atmospheres. The μ_{FE} increases with the Ar/O_2, reaching a peak, and then exhibits a slight decrease after saturation. Notably, when the Ar/O_2 increases from 20/30 sccm to 30/20 sccm, there is a significant increase in μ_{FE}. This increase in μ_{FE} may be related to the decrease in the proportion of oxygen in the sputtering atmosphere, which leads to an increase in the number of V_os inside the active layer [15], [29].

Fig. 4c shows the extracted V_{th} of IZO TFTs with different sputtering atmospheres. The V_{th} is closely related to the sputtering atmospheres. As the Ar/O_2 increases from 20/30 sccm to 40/10 sccm, the V_{th} of the device gradually deviates from 0 V, showing a negative shift trend. Among all devices, the optimal V_{th} is ~0V. The increase in V_os content in the active layer caused by a lower oxygen concentration in the sputtering atmosphere may be responsible [29]. The increase in V_os leads to a higher number of carriers, making it easier for free charge carriers to accumulate in the transport layer, thereby facilitating the operation of the device.

Fig. 4d shows the extracted *SS* of IZO TFTs with different sputtering atmospheres. As the Ar/O_2 increases, the *SS* initially decreases and then increases. At Ar/O_2 = 30/20 sccm, the minimum *SS* is ~0.1 mV/dec. An appropriate sputtering atmosphere can maintain the *SS* of the device in a relatively optimal state, while excessive or insufficient Ar/O_2 may lead to the deterioration of *SS*. This deterioration may be related to both the internal defect state of the film [29] and/or changes in the surface roughness of the film [30].

The performance variations of IZO TFTs with changes in IZO thickness and sputtering atmosphere suggest that V_os/defect states within the channel and the surface roughness of the active layer are key factors affecting device performance. To better confirm these relationships, AFM and XPS analyses were performed.

Shown in Fig. 5a to 5d are AFM images of IZO thin film with different thicknesses. The root mean square roughness (R_q) of 4.8 nm IZO thin film, 9.7 nm IZO thin film, 24 nm IZO thin film, and 36 nm IZO thin film is respectively 0.304 nm, 0.321 nm, 0.426 nm, and 0.477 nm. The surface roughness of the IZO film increases with thickness. The surface roughness mainly affects the interface quality and therefore affects the *SS*. When the film is thin (< 14.5 nm), *SS* deteriorates with the decrease of thickness (Fig. 3d) due to the increase of R_q. Since the active layer is thin, the carrier transport layer is a relatively fixed area near the interface, which amplifies the impact of interface defects on the device performance [26]. When the film becomes thick (> 14.5 nm), Although R_q decreases with the increase of thickness, the *SS* still slightly deteriorates (Fig. 3d), which can be explained by the increase of sheet trap density and the decrease of effective capacitance at the interface in the thick active thin film [28].

Fig. 5e to 5f are AFM images of IZO thin film with different Ar/O_2. The R_q of IZO thin film fabricated at Ar/O_2= 20/30 sccm, 30/20 sccm, 35/15 sccm, and 40/10 sccm are respectively 0.318 nm, 0.339 nm, 0.349 nm, and 0.421 nm. The surface roughness of the IZO film also increases with Ar/O_2. The increase in surface roughness indicates a lower film density and deterioration of the interface state [31]. Additionally, it leads to an increase in contact resistance between the channel and the source/drain electrodes [30]. Lower film density, worse interface quality, and larger contact resistance jointly cause *SS* deterioration with increasing Ar/O_2 (Fig. 4d) and hinder carrier flow in the transport layer, thereby limiting μ_{FE} improvement.

The binding energy of thin films produced under different conditions is characterized by XPS. Calibrating with the C1s peak at 284.8 eV, the O1s peak is decomposed into three subpeaks with binding energy centers at 530 ± 0.5

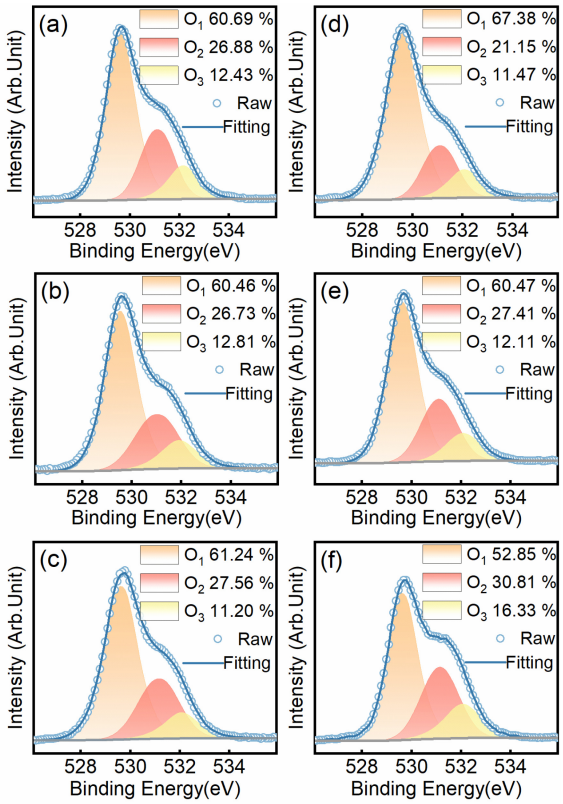

FIGURE 6. XPS images of IZO thin film with (a) IZO thickness of 9.7 nm, (b) IZO thickness of 24 nm, and (c) IZO thickness of 36 nm. XPS images of IZO thin film fabricated at (d) Ar/O_2 = 20/30 sccm, (e) Ar/O_2 = 30/20 sccm, and (f) Ar/O_2 =40/10 sccm.

eV (peak 1), 531 ± 0.5 eV (peak 2), and 532 ± 0.5 eV (peak 3), as shown in Fig. 6 Peak 1 typically represents a metal–oxygen (M–O) bond, peak 2 represents V_os, and peak 3 impurities related to oxygen, such as –OH, adsorbed oxygen, and $-CO_3^{2-}$[2]. As shown in Fig. 6a to 6c, the XPS spectra of devices with different IZO thicknesses reveal no significant fluctuation in the percentage content of the three oxygen peaks, indicating that IZO thickness is not a critical factor affecting the relative content of V_os.

Compared to Fig. 6a to 6c, the fluctuation of the oxygen peaks in Fig. 6d to 6f is more pronounced. When Ar/O_2 increases from 20/30 sccm to 40/10 sccm, the relative content of V_os (peak 2) rises from 21.15% to 30.81%. Additionally, oxygen–related impurities (peak 3) increase to 16.33%. A high oxygen atmosphere leads to more V_os repair. In MO TFTs, V_os can convert into electrons, enhancing device μ_{FE} [17], [32]. The specific conversion process is shown in the following equation [32],

$$(\mathrm{V_o}) \leftrightarrow \mathrm{V_o^{2-}} + 2\mathrm{e^-}$$

where V_o^{2-} stands for divalent oxygen vacancy (V_o). In an oxygen-rich sputtering atmosphere, excess oxygen acts as acceptor defects in the film, binding with free carriers and reducing mobility [32]. This explains the decreasing device μ_{FE} as Ar/O_2 decreases in Fig. 4b. Conversely, in an oxygen-deficient atmosphere, abundant V_os increase carriers, leading

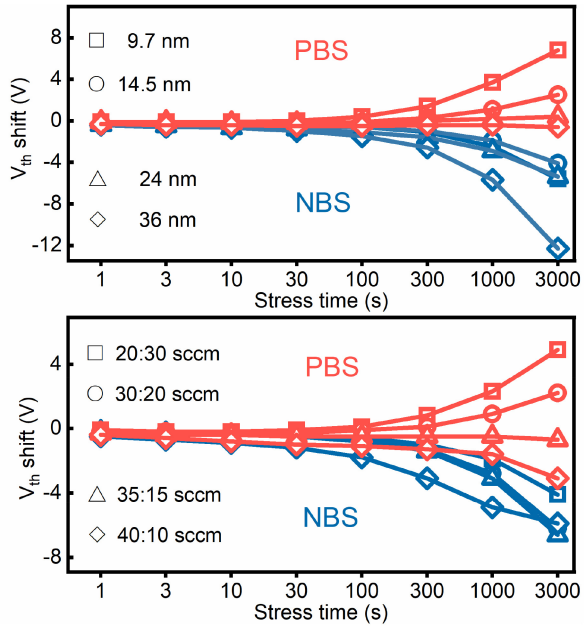

FIGURE 7. (a) V_{th} shift dependent on stress time in IZO TFTs with different IZO thicknesses under P/NBS. (b) V_{th} shift dependent on stress time in IZO TFTs fabricated at different Ar/O_2 under P/NBS.

to a negative shift in V_{th} (Fig. 4c) and improved device μ_{FE} (Fig. 4d). Hence, the selection of the appropriate Ar/O_2 ratio is pivotal in the fabrication of devices characterized by high μ_{FE} and favorable V_{th}. Additionally, the escalating trend observed in the peak3 with increasing Ar/O_2 suggests that the active layer sputtered under anaerobic conditions contains greater quantities of impurities. This phenomenon significantly contributes to the degradation of *SS* observed in Fig. 4d as Ar/O_2 increases.

The impact of different manufacturing processes on device reliability is also investigated. Shown in Fig. 7a is the V_{th} shift dependent on stress time under NBS and PBS in IZO TFTs with different IZO thicknesses and shown in Fig. 7b is the V_{th} shift dependent on stress time under NBS and PBS in IZO TFTs fabricated at different Ar/O_2.

For PBS, it can be observed that IZO TFTs with a small IZO thickness (Fig. 7a) and IZO TFTs fabricated at low Ar/O_2 (Fig. 7b) experience a positive shift in V_{th} while IZO TFTs with a large IZO thickness (Fig. 7a) and IZO TFTs fabricated at high Ar/O_2 (Fig. 7b) experience a negative shift to some degree. For PBS-induced degradation in MO TFTs, there are three dominant effects, namely charge trapping [33], [34], oxygen adsorption [35], and V_os redistribution [36]. Charge trapping and oxygen adsorption leads to a positive V_{th} shift while V_os redistribution leads to a negative V_{th} shift [33], [34], [35], [36]. According to Fig. 6, the large IZO thickness and the low oxygen atmosphere during sputtering result in a higher amount of V_os, which leads to the dominant redistribution of V_os under long-term PBS, resulting in a negative shift in V_{th}. On the contrary, the small IZO thickness and high oxygen atmosphere during sputtering result in less V_os. Under PBS, the redistribution

mechanism of V_os is gradually surpassed by the other two mechanisms, ultimately leading to a positive shift of V_{th}.

Under NBS, V_{th} exhibits a negative shift trend, especially for devices with large IZO thickness and high Ar/O_2. For NBS-induced degradation in MO TFTs, there are two dominant effects, namely V_os ionization [24] and interaction between charge carriers in the channel and impurities in the environment [37]. Large thickness and high Ar/O_2 lead to an increase in V_os ionization caused by excessive V_os. In addition, according to Figure 4e to h, the reduction of oxygen in the sputtering atmosphere leads to an increase in the surface roughness of the channel. The increase in surface roughness may indicate that the channel has a stronger adsorption effect on external moisture. As shown in Figure 5 d to f, as the Ar/O_2 increases, the relative content of peak 3, which represents weak oxygen binding bonds, increases, indicating that more moisture adsorption reactions occur at the channel interface. Therefore, NBS degradation is more severe in devices with large IZO thickness and high Ar/O_2.

IV. CONCLUSION

In this study, RF magnetron sputtering was employed to optimize IZO TFTs through a systematic approach. By jointly tuning the annealing condition, IZO thickness, and Ar/O_2, high-performance IZO TFTs with μ_{FE} of ~71.8 cm^2/Vs with a V_{th} of ~–0.6 V are achieved. Furthermore, the reliability of the corresponding IZO TFTs under PBS and NBS is also examined. This comprehensive investigation aims to offer valuable insights for advancing the development of high-performance MO TFTs.

REFERENCES

[1] J.-S. Seo and B.-S. Bae, "Improved electrical performance and bias stability of solution-processed active bilayer structure of indium zinc oxide based TFT," *ACS Appl. Mater. Interfaces*, vol. 6, no. 17, pp. 15335–15343, Sep. 2014, doi: 10.1021/am5037934.
[2] W. Yang, H. Yang, J. Su, and X. Zhang, "Preparation and electrical characteristics of Li–N co-doped InZnAlO thin film transistors by radio frequency magnetron sputtering," *Vacuum*, vol. 205, Nov. 2022, Art. no. 111419, doi: 10.1016/j.vacuum.2022.111419.
[3] Y. J. Im, S. J. Kim, J. H. Shin, S. S. Ha, C. H. Park, and M. Yi, "Improvement in the electrical performance of Ge-doped InZnO thin-film transistor," *J. Nanosci. Nanotechnol.*, vol. 15, no. 10, pp. 7537–7541, Oct. 2015, doi: 10.1166/jnn.2015.11156.
[4] Z. Pan et al., "Approaches to improve mobility and stability of IGZO TFTs: A brief review," *Trans. Electr. Electron. Mater.*, vol. 25, pp. 371–379, Apr. 2024, doi: 10.1007/s42341-024-00536-1.
[5] S. Park, K. Park, H. Kim, H.-W. Park, K.-B. Chung, and J.-Y. Kwon, "Light-induced bias stability of crystalline indium-tin-zinc-oxide thin film transistors," *Appl. Surf. Sci.*, vol. 526, Oct. 2020, Art. no. 146655, doi: 10.1016/j.apsusc.2020.146655.
[6] P.-T. Liu, P.-Y. Kuo, and S.-M. Hsu, "(Invited) high performance amorphous In-W-Zn-O thin film transistor with ultra-thin active channel for low voltage operation," *ECS Trans.*, vol. 86, no. 11, pp. 91–93, Jul. 2018, doi: 10.1149/08611.0091ecst.
[7] C. A. Hoel, J.-F. Gaillard, and K. R. Poeppelmeier, "Probing the local structure of crystalline ZITO: In2-2xSnxZnxO3 (x≤0.4)," *J. Solid State Chem.*, vol. 183, no. 4, pp. 761–768, Apr. 2010, doi: 10.1016/j.jssc.2010.01.014.
[8] R. N. Chauhan and N. Tiwari, "Zinc oxide incorporated indium tungsten oxide amorphous thin films for thin film transistors applications," *J. Non-Cryst. Solids*, vol. 556, Mar. 2021, Art. no. 120556, doi: 10.1016/j.jnoncrysol.2020.120556.
[9] M. Fujii et al., "Low temperature high-mobility InZnO thin-film transistors fabricated by excimer laser annealing," *Appl. Phys. Lett.*, vol. 102, no. 12, Mar. 2013, Art. no. 122107, doi: 10.1063/1.4798519.
[10] G. Socol et al., "Pulsed laser deposition of transparent conductive oxide thin films on flexible substrates," *Appl. Surf. Sci.*, vol. 260, pp. 42–46, Nov. 2012, doi: 10.1016/j.apsusc.2012.02.148.
[11] Y.-K. Liang et al., "Electrical characteristics of ultrathin InZnO thin-film transistors prepared by atomic layer deposition," *IEEE Trans. Electron Devices*, vol. 70, no. 3, pp. 1067–1072, Mar. 2023, doi: 10.1109/TED.2022.3232476.
[12] S. Lee et al., "Patterned oxide semiconductor by electrohydrodynamic jet printing for transparent thin film transistors," *Appl. Phys. Lett.*, vol. 100, no. 10, Mar. 2012, Art. no. 102108, doi: 10.1063/1.3691177.
[13] P. Barquinha, A. Pimentel, A. Marques, L. Pereira, R. Martins, and E. Fortunato, "Influence of the semiconductor thickness on the electrical properties of transparent TFTs based on indium zinc oxide," *J. Non-Cryst. Solids*, vol. 352, nos. 9–20, pp. 1749–1752, Jun. 2006, doi: 10.1016/j.jnoncrysol.2006.01.067.
[14] Z. Yang, J. Yang, T. Meng, M. Qu, and Q. Zhang, "Influence of channel layer thickness on the stability of amorphous indium zinc oxide thin film transistors," *Mater. Lett.*, vol. 166, pp. 46–50, Mar. 2016, doi: 10.1016/j.matlet.2015.12.029.
[15] A. S. Reed, D. C. Paine, and S. Lee, "Effect of O2 fraction in the sputter gas on the electrical properties of amorphous In-Zn-O and the thin film transistor performance," *J. Electron. Mater.*, vol. 45, no. 12, pp. 6310–6316, Dec. 2016, doi: 10.1007/s11664-016-5008-1.
[16] P. Barquinha, G. Gonçalves, L. Pereira, R. Martins, and E. Fortunato, "Effect of annealing temperature on the properties of IZO films and IZO based transparent TFTs," *Thin Solid Films*, vol. 515, no. 24, pp. 8450–8454, Oct. 2007, doi: 10.1016/j.tsf.2007.03.176.
[17] J. S. Park, W.-J. Maeng, H.-S. Kim, and J.-S. Park, "Review of recent developments in amorphous oxide semiconductor thin-film transistor devices," *Thin Solid Films*, vol. 520, no. 6, pp. 1679–1693, Jan. 2012, doi: 10.1016/j.tsf.2011.07.018.
[18] M. M. Billah et al., "High-performance coplanar dual-channel a-InGaZnO/a-InZnO semiconductor thin-film transistors with high field-effect mobility," *Adv. Electron. Mater.*, vol. 7, no. 3, Mar. 2021, Art. no. 2000896, doi: 10.1002/aelm.202000896.
[19] Y. Han, H. Yan, Y.-C. Tsai, Y. Li, Q. Zhang, and H.-P. D. Shieh, "Influences of nitrogen doping on the electrical characteristics of indium-zinc-oxide thin film transistors," *IEEE Trans. Device Mater. Reliab.*, vol. 16, no. 4, pp. 642–646, Dec. 2016, doi: 10.1109/TDMR.2016.2617336.
[20] S.-H. Lee, S.-Y. Bak, and M. Yi, "Improved performance and bias stability of Al2O3/IZO thin-film transistors with vertical diffusion," *Electronics*, vol. 11, no. 14, p. 2263, Jul. 2022, doi: 10.3390/electronics11142263.
[21] I. H. Kim, S. J. Kim, S.-J. Kim, T. K. An, and Y. J. Jeong, "The impact of nickel doping on metal-oxide network in solution-processed indium zinc oxide transistors," *Mater. Today Commun.*, vol. 35, Jun. 2023, Art. no. 106221, doi: 10.1016/j.mtcomm.2023.106221.
[22] D. Lin, K. Li, J. Shao, and Q. Zhang, "High-performance thin-film transistors with nickel-doped indium zinc oxide channel layers," *Phys. Status Solidi A*, vol. 216, no. 18, Sep. 2019, Art. no. 1900274, doi: 10.1002/pssa.201900274.
[23] X. Ding et al., "Growth of IZO/IGZO dual-active-layer for low-voltage-drive and high-mobility thin film transistors based on an ALD grown Al2O3 gate insulator," *Superlattices Microstruct.*, vol. 76, pp. 156–162, Dec. 2014, doi: 10.1016/j.spmi.2014.10.007.
[24] J. Park, Y. Lim, M. Jang, S. Choi, N. Hwang, and M. Yi, "Improved stability of aluminum co-sputtered indium zinc oxide thin-film transistor," *Mater. Res. Bull.*, vol. 96, pp. 155–159, Dec. 2017, doi: 10.1016/j.materresbull.2017.05.001.
[25] C. Park et al., "Effect on electrical performance of titanium co-sputtered IZO active-channel thin-film transistor," *J. Soc. Inf. Disp.*, vol. 23, no. 8, pp. 371–376, Aug. 2015, doi: 10.1002/jsid.321.
[26] A. H. Chen et al., "Influence of the channel layer thickness on electrical properties of indium zinc oxide thin-film transistor," *Microelectron. Eng.*, vol. 87, no. 10, pp. 2019–2023, Oct. 2010, doi: 10.1016/j.mee.2009.12.081.
[27] J.-S. Park, J. K. Jeong, Y.-G. Mo, H. D. Kim, and C.-J. Kim, "Control of threshold voltage in ZnO-based oxide thin film transistors," *Appl. Phys. Lett.*, vol. 93, no. 3, Jul. 2008, Art. no. 33513, doi: 10.1063/1.2963978.

[28] Y. Wang, X. W. Sun, G. K. L. Goh, H. V. Demir, and H. Y. Yu, "Influence of channel layer thickness on the electrical performances of inkjet-printed In-Ga-Zn Oxide thin-film transistors," *IEEE Trans. Electron Devices*, vol. 58, no. 2, pp. 480–485, Feb. 2011, doi: 10.1109/TED.2010.2091131.

[29] C. Fan, Y. Xin, L. Qin, X. Zhou, and S. Zhang, "P-45: Effect of Ar / O 2 flow ratio during sputtering of InZnO active layer on photocurrent and responsivity characteristics of amorphous InZnO thin film transistors," in *SID Symp. Dig. Tech. Paper*, 2020, pp. 1515–1518, doi: 10.1002/sdtp.14176.

[30] E. Crinon and J. T. Evans, "The effect of surface roughness, oxide film thickness and interfacial sliding on the electrical contact resistance of aluminium," *Mater. Sci. Eng. A*, vol. 242, pp. 121–128, Feb. 1998.

[31] H.-W. Park, K. Park, J.-Y. Kwon, D. Choi, and K.-B. Chung, "Effect of active layer thickness on device performance of tungsten-doped InZnO thin-film transistor," *IEEE Trans. Electron Devices*, vol. 64, no. 1, pp. 159–163, Jan. 2017, doi: 10.1109/TED.2016.2630043.

[32] H. Duan, L. Liang, Z. Wu, H. Zhang, L. Huang, and H. Cao, "IGZO/CsPbBr 3 -nanoparticles/IGZO neuromorphic phototransistors and their optoelectronic coupling applications," *ACS Appl. Mater. Interfaces*, vol. 13, no. 25, pp. 30165–30173, Jun. 2021, doi: 10.1021/acsami.1c05396.

[33] E. N. Cho, J. H. Kang, C. E. Kim, P. Moon, and I. Yun, "Analysis of bias stress instability in amorphous InGaZnO thin-film transistors," *IEEE Trans. Device Mater. Reliab.*, vol. 11, no. 1, pp. 112–117, Mar. 2011, doi: 10.1109/TDMR.2010.2096508.

[34] M. G. Yun, S. H. Kim, C. H. Ahn, S. W. Cho, and H. K. Cho, "Effects of channel thickness on electrical properties and stability of zinc tin oxide thin-film transistors," *J. Phys. Appl. Phys.*, vol. 46, no. 47, Nov. 2013, Art. no. 475106, doi: 10.1088/0022-3727/46/47/475106.

[35] D. Kang et al., "Amorphous gallium indium zinc oxide thin film transistors: Sensitive to oxygen molecules," *Appl. Phys. Lett.*, vol. 90, no. 19, May 2007, Art. no. 192101, doi: 10.1063/1.2723543.

[36] Y. Yang, D. Zhang, M. Wang, L. Lu, and M. Wong, "Suppressed degradation of elevated-metal metal–oxide thin-film transistors under bipolar gate pulse stress," *IEEE Electron Device Lett.*, vol. 39, no. 5, pp. 707–710, May 2018, doi: 10.1109/LED.2018.2821366.

[37] H. Xie, Q. Wu, L. Xu, L. Zhang, G. Liu, and C. Dong, "Nitrogen-doped amorphous oxide semiconductor thin film transistors with double-stacked channel layers," *Appl. Surf. Sci.*, vol. 387, pp. 237–243, Nov. 2016, doi: 10.1016/j.apsusc.2016.05.116.